HOKKAIDO UNIVERSITY

Title	Silver-doped TiO2 prepared by microemulsion method: Surface properties, bio- and photoactivity
Author(s)	Zielińska, Anna; Kowalska, Ewa; Sobczak, Janusz W.; Łącka, Izabela; Gazda, Maria; Ohtani, Bunsho; Hupka, Jan; Zaleska, Adriana
Citation	Separation and Purification Technology, 72(3), 309-318 https://doi.org/10.1016/j.seppur.2010.03.002
Issue Date	2010-05-11
Doc URL	http://hdl.handle.net/2115/48658
Type	article (author version)
File Information	SPT2010_Ohtani.pdf

Instructions for use

Silver-doped TiO$_2$ prepared by microemulsion method: surface properties, bio- and photoactivity

Anna Zielińska[a], Ewa Kowalska[a,e,f], Janusz W. Sobczak[d], Izabela Łącka[b], Maria Gazda[c],
Bunsho Ohtani[e], Jan Hupka[a], Adriana Zaleska[1a]

[a]*Department of Chemical Technology, Faculty of Chemistry,*

[b]*Department of Pharmaceutical Technology and Biochemistry, Faculty of Chemistry*

[c]*Department of Solid State Physics, Faculty of Applied Physics and Mathematics*

Gdansk University of Technology, 80-233 Gdansk, Poland

[d]*Laboratory of Electron Spectroscopies, Institute of Physical Chemistry, Polish Academy*
of Sciences, 01-224 Warsaw, Poland

[e]*Catalysis Research Center, Hokkaido University, Sapporo 001-0021, Japan,*

[f]*Friedrich Alexander Universität Erlangen-Nürnberg, Institut für Anorganische Chemie,*
91058 Erlangen, Germany

Abstract

A series of Ag-TiO$_2$ photocatalysts were obtained in microemulsion system (water/AOT/cyclohexane), using several Ag precursor amount ranging from 1.5 to 8.5 mol.%. The photocatalysts' characteristics by X-ray diffraction, STEM microscopy, UV-Vis spectroscopy, X-ray photoelectron spectroscopy, BET methods showed that a sample with the highest photo- and bioactivity had anatase structure, about 90 m^2/g specific surface area, absorbed light for λ>400 nm and contained 1.64 at.% of silver (0.30 at.% of Ag^0 and 1.34 at.% of Ag$_2$O) and about 13 at.% of carbon in the surface layer. The photocatalytic activity of the catalysts was estimated by measuring the decomposition rate of phenol in 0.21 mM aqueous solution under visible and ultraviolet light irradiation. The bioactivity of silver-doped titanium dioxide nanocomposites was estimated using bacteria *Escherichia coli* and *Staphylococcus aureus*, yeast *Saccharomyces cerevisiae* and pathogenic fungi belonging to *Candida* family. All modified powders showed localized surface plasmon resonance (LSPR) in visible region with almost the same position of LSPR peaks indicating that similar sizes of silver, regardless of used amount of Ag, is deposited on titania particles during microemulsion method. STEM microscopy revealed

---

[1] Author to whom correspondence should be addressed. E-mail: adriana.zaleska@pg.gda.pl, tel: 48 58 3472437, fax: 48 58 3472065, ul. Narutowicza 11/12, 80-233 Gdansk, Poland

that almost 50% of observed silver nanoparticles deposited at the TiO_2 surface are in the range from 5 to 10 nm.

1. Introduction

Silver doped titanium dioxide nanoparticles became of current interests because of both their effects on the improvement of photocatalytic activity of TiO_2 and their effects on antibacterial activity. Noble metals deposited or doped with TiO_2 have high Schottky barriers among the metals and thus act as electron traps, facilitating electron–hole separation and promote the interfacial electron transfer process [1-2]. Silver can trap the excited electrons from titanium dioxide and leave the holes for the degradation reaction of organic species. It also results in the extension of their wavelength response towards the visible region [3]. In addition, silver nanoparticles possess the ability to absorb visible light, due to localized surface plasmon resonance (LSPR) [4]. These properties have led to tremendous range of applications of Ag-TiO_2 nanoparticles, for instance, antibacterial textiles, engineering materials, medical devices, food preparation surfaces, air conditioning filters and coated sanitary wares.

The conventional method that has been applied to prepare Ag-TiO_2 nanoparticles is sol-gel process with chemical, thermal or photochemical reduction of silver ions. Several approaches to Ag-TiO_2 preparation have been proposed: one-step sol-gel route [5-9], photoreduction of Ag^+ in TiO_2 suspension [10] and by electrochemical deposition of Ag nanoparticles at the TiO_2 surface [11]. Kawahara et al. [11] found that photochemically and electrochemically deposited silver exhibits multicolor photochromism in the nanoporous TiO_2 film. The multicolor photochromism is not generally observed for silver nanoparticles, because in the photo-oxidation process the TiO_2 matrix plays an important role. The photo-excited electrons on silver are transferred to oxygen molecules via titanium dioxide and non-excited silver [11].

Tran et al. [12] stated that the presence of silver mainly enhances the photocatalytic oxidation of organic compounds that are predominantly oxidized by holes, while it has not insignificant effect on those organic compounds that require hydroxyl radicals for their mineralization. They found that the enhancing effect of silver deposits on TiO_2 can initially by predicted by the molecular structure of the substrate to be oxidized. The fewer C-H bonds and/or more C=O and C-O bonds a molecule possesses, the more probable the enhancement of mineralization in the presence of silver.

Hamal et al. [13] reported the synthesis and characterization of highly active (in visible light) new nanoparticle photocatalysts based on silver, carbon and sulfur-doped TiO_2 prepared by sol-gel route. They found that Ag/(C, S)–TiO_2 nanoparticle photocatalysts degrade the gaseous acetaldehyde 10 and 3 times faster than P25–TiO_2 under visible and UV light, respectively [13].

Although the precipitation technique is easy, the morphology and the size of the obtained Ag/TiO_2 nanoparticles are difficult to control, which results in unreliable properties in real applications. Compared with these methods, the preparation of silver doped titanium dioxide nanoparticles in w/o microemulsion offers a unique microenvironment in which monodispersed, ultrafine Ag/TiO_2 nanoparticles with a narrow size distribution can be obtained. This method has obvious advantages of obtaining nanoparticles with specific diameter and morphology. Water microdroplets surrounded by a monolayer of surfactant in a continuous hydrocarbon phase act as microreactors to synthesize nanoparticles whose growing is controlled inside the water droplet giving rise to a narrow size distribution [14]. Inaba et al. [15] prepared titanium dioxide nanoparticles in a reverse micelle system composed of water, Triton X-100 and isooctane. The TiO_2 nanoparticles showed monodispersity, a large surface area and high degrees of crystallinity and thermostability. The particle size of TiO_2 was controlled by changing the water content of the reverse micelle solution [15]. A reverse micelle system is also favorable for preparation of nanosilver particles with narrow size distribution. Zhang et al. [14] reported that silver nanoparticles prepared in AOT microemulsion have a smaller average size and a narrower size distribution compared to the particles prepared by using cationic or nonionic surfactant in microemulsion system. In our previous work we also studied the preparation of silver nanoparticles in water/AOT/dodecane microemulsion [16]. We obtained stable monodisperse silver nanoparticles with a narrow size distribution. The diameter size of the silver nanoparticles was in the range 5-10 nm [17]. Based on literature data, microemulsion appears as favorable environment for nanoparticles preparation, but Ag-TiO_2 preparation in the microemulsion system has not been investigated.

The aim of this study was to investigate a reverse micelle system for Ag-TiO_2 nanocomposites synthesis and to characterize the obtained nanoparticles. Here we report the preparation method of silver doped titanium dioxide nanoparticles in the water-in-oil microemulsion system of water/AOT/cyclohexane. Sodium bis (2-ethylhexyl) sulfosuccinate (AOT), as the most common surfactant used to form reverse micelles, were chosen for our investigation. The effect of silver content used for preparation on the

photocatalyst structure, surface area, crystallinity, and efficiency of removal of model organic compound and model microorganisms from aqueous phase were systematically investigated.

2. Experimental

2.1. Materials and instruments

Titanium isopropoxide (pure p.a.) was purchased from Aldrich and used as titanium source for the preparation of TiO_2 nanoparticles. A commercial form of TiO_2 (P25, ca. 80% anatase, 20% rutile) from Degussa was used for the comparison of the photocatalytic activity. Silver nitrate (pure p.a.) was provided by POCh and used as the starting material for the silver nanoparticles. Hydrazine anhydrous and ascorbic acid (99%) were purchased from Aldrich and used as reducing agents. Cyclohexane was used as the continuous oil phase, and sodium bis- (2-ethylhexyl) sulfosuccinate (AOT) purchased from Aldrich as the surfactant, and aqueous solution as the dispersed phase, without addition of any co-surfactant.

The crystal structures of the Ag-TiO_2 nanoparticles were determined from XRD pattern measured in the range of $2\theta = 20$–80° using X-ray diffractometer (Xpert PRO-MPD, Philips) with Cu target ($\lambda = 1.542$ Å). The XRD estimation of the crystallite size was based on the Scherrer formula: $d = \dfrac{0.89\,\lambda}{(B_e - B_t) \cdot \cos\theta}$, where λ is the X-ray wavelength, B_e indicates the measured breadth of a peak profile, while B_t is the ideal, non-broadened breadth of a peak and θ is the diffraction angle. The value of B_t was estimated on the basis of the measurements performed for a standard sample of polycrystalline Si with large crystalline grains. The accuracy of the grain size analysis has been estimated to be about 20 %.

To characterize the light-absorption properties of modified photocatalysts, diffuse reflectance (DR) spectra were recorded, and data were converted to obtain absorption spectra. The measurements were carried out on Jasco V-670 spectrophotometer equipped with a PIN-757 integrating sphere where the baseline was recorded using a poly(tetrafluoroethylene) reference and bare titania powders.

Nitrogen adsorption–desorption isotherms were recorded at liquid nitrogen temperature (77 K) on a Micromeritics Gemini V (model 2365) and the specific surface areas were determined by the Brunauer–Emmett–Teller (BET) method.

The morphology of silver photodeposited onto titania was observed by Scanning Transmission Electron Microscopy (STEM, Hitachi, HD2000 ultrathin film evaluation system). Secondary electron (SE), Z-contrast (ZC) and bright-field (BF) STEM were recorded. Ag/TiO_2 powders were dispersed in ethanol in an ultrasound bath for a few minutes. Some drops of suspension were deposited on carbon covered microgrid. The images were acquired at wide range of magnification (200.000-180.000.000) in normal, high resolution and ultra high resolution modes using 3 and 2 mm working distance, 200 kV accelerating voltage and 30 μA emission current.

All XPS spectra were recorded on a Physical Electronics PHI 5000 Versa Probe scanning spectrometer using monochromatic Al Ka X-rays working with power 25 W. X-ray beam was focused to diameter 100 μm, measured area was defined as 250 x 250 μm. The hemispherical electron energy analyzer was operated at a pass energy 23.50 eV for all high resolution measurements. All measurements were conducted with the use of a neutralizer working both with low energy electrons and low energy Ar^+ ions. A PHI Multipak software was used to evaluate the XPS data (Shirley type background subtraction). For final calibration of spectra the peak $Ti2p_{3/2}$ of TiO_2 support was used with BE values =458.60 eV.

2.2 Preparation of Ag-doped TiO$_2$ photocatalysts

Silver doped titanium dioxide nanoparticles were prepared by adding titanium tetraisopropoxide (TIP) dropwise into the microemulsion containing silver precursor in water cores [16]. Water content was controlled by fixing the molar ratio of water to surfactant (w_o) at 2. Mixing was carried out for 2h and then the silver ions adsorbed on titanium dioxide were reduced to elemental silver by dropwise addition microemulsion containing a reducing agent (hydrazine or ascorbic acid). During the precipitation nitrogen was bubbled continuously through the solution. The Ag/TiO_2 particles precipitated were separated in a centrifuge at 2000 rpm for 2 min and were then washed with ethanol and deionized water several times to remove the organic contaminants and surfactant. The particles were dried at 80°C for 48 h and were then calcinated at 450°C for 2h. The schematic illustration of the preparation method of silver doped titanium dioxide nanoparticles in reverse micelles is presented in Fig. 1.

As reference samples, pure TiO_2 and Degussa P25 loaded with 6.5 mol.% were prepared. To evaluate the effect of microemulsion method on titanium dioxide structure, pure TiO_2 was obtained by TIP hydrolysis in the microemulsion system followed by separation, washing, drying and calcination at 450 °C. Silver deposited at the surface of P25 TiO_2

nanoparticles was obtained by mixing microemulsion containing P25 TiO_2 and Ag ions with microemulsion containing ascorbic acid in the N_2 atmosphere. The obtained photocatalyst was separated, washed and dried at 80°C for 48 h and then calcinated at 450°C for 2h.

2.3. Measurements of photocatalytic activity

The photocatalytic activity of Ag-TiO_2 powders under UV and visible light was estimated by measuring the decomposition rate of phenol (0.21 mmol/dm^3) in an aqueous solution. Photocatalytic degradation runs were preceded by blind tests in the absence of a photocatalyst or illumination. Phenol was selected as a model pollutant because it is a non-volatile and common contaminant present in industrial wastewaters. The mechanism of phenol decomposition is also well established. 25ml of phenol solution at concentration of $2.1 \cdot 10^{-4}$ M containing suspended photocatalyst (125 mg) was stirred using a magnetic stirrer and aerated (5 dm^3/h) prior and during the photocatalytic process. Aliquots of 1.0 cm^3 of the aqueous suspension were collected at regular time periods during irradiation and filtered through syringe filters (Ø = 0.2 μm) to remove photocatalyst particles. Phenol concentration was estimated by colorimetric method using UV–vis spectrophotometer (DU-7, Beckman). The suspension was irradiated using 1000 W Xenon lamp (6271H, Oriel), which emits both UV and vis light. The optical path included water filter and glass filters (GG400 or UG1, Schott AG) to cut off IR and VIS or UV irradiation, respectively. GG glass filter transmitted light of wavelength greater than 400 nm, whereas UG in the range of 250÷400 nm (max. 330 nm). The temperature during the experiments was maintained at 10°C.

2.4. Measurements of bioactivity (antibacterial and antifungal)

MIC (minimal inhibitory concentration)

Antibacterial and antifungal activity was determined by the serial twofold dilution microtiter plate method, in Tryptic Soy Broth medium (TSB, GibcoBRL), for antibacterial activity determination or in YNBG medium (Yeast Nitrogen Base-glucose minimal medium, containing 0,67 % YNB without amino acids and ammonium sulphate with addition of 2 % glucose and 5 g/l of ammonium sulphate, supplemented with uracil at 30 μg/l) for antifungal activity determination. Wells containing serially diluted examined compounds (suspended Ag-TiO_2) and compound-free controls were inoculated with overnight cultures of tested strains to the final concentration of 10^4 cfu/ml (colony forming units per ml). The plates were then incubated for 24 h at 37°C (antibacterial activity determination) or at 30°C (antifungal activity determination). The microbial growth was

quantified in each well by the measurement of an optical density at $\lambda = 531\text{nm}$ using the microplate reader (Victor[3]V, PerkinElmer, Centre of Excellence ChemBioFarm, Faculty of Chemistry, Gdansk University of Technology). MIC (minimal inhibitory concentration) was defined as drug concentration at which at least 80 % decrease in turbidity, relative to that of the compound-free growth control well was found. The antimicrobial activity of silver-doped titanium dioxide nanocomposites was estimated using *Escherichia coli* ATCC 10536*, Staphylococcus aureus* ATCC 6538*, Candida albicans* ATCC 10231*, Candida glabrata* DSM 11226, *Candida tropicalis* KKP 334, *Saccharomyces cerevisiae* ATCC 9763, *S. cerevisiae* JG and JG CDR1.

Zones of inhibition.

The solid YEPG (2% glucose, 1% yeast extract, 1% bacto-peptone, 2% agar, for fungi) or Tryptic Soy Agar (BTL, for bacteria) were liquefied by warming at 100°C and then chilled to 40°C. The semi-liquid medium was inoculated with 3×10^5 cells/ml of an overnight culture of microbial cells, poured into Petri plates and left for solidification. The Ag-TiO$_2$ nanoparticles were suspended in dimethyl sulfoxide (DMSO) to create a concentration of 4 mg/ml. 20 μl of this suspension were spotted onto the agar medium surface (diameter of each spot ∼ 9 mm, three spots on each plate). The plates were incubated for 24 h at 37° C (antibacterial activity determination) or at 30°C (antifungal activity determination). Growth inhibition zones appearing around the spots were measured.

3. Results and discussion

3.1. Photocatalytic activity of pure TiO$_2$ and Ag-doped TiO$_2$ under UV and visible light

The photocatalytic activity of the as-prepared nanocomposites was studied by examining the reaction of phenol degradation. No phenol was degraded in the absence of illumination indicating that there was no dark reaction at the surface of Ag-TiO$_2$. Also the reference test in the absence of photocatalysts under visible light showed the lack of phenol degradation. Sample labeling, silver amount and reducing agent used in the preparation procedure, as well as photocatalysts characteristics are given in Table 1. Pure TiO$_2$, prepared by the same microemulsion method without adding of Ag$^+$ and reducing agent solutions, was used as a reference sample. The efficiency of phenol degradation after 80 min. illumination by UV or visible light in the presence of pure TiO$_2$ and Ag-doped TiO$_2$ are presented in Table 1 and Fig. 2.

Compared to pure TiO$_2$, the TiO$_2$ loaded with 4.5, 6.5 and 8.5 mol.% of Ag exhibited a significant increase in the UV-driven phenol degradation rate as shown in Table 1 and

Fig. 2a. The maximum in the photocatalytic activity under UV light irradiation was observed for 6.5 mol % Ag doped TiO_2. After 80 min of irradiation about 86% of phenol was degraded. The efficiency decreased to 76 and 81% for the Ag-TiO_2 4.5% and Ag-TiO_2 8.5% photocatalysts, respectively. The lowest photoactivity (32%) revealed undoped TiO_2 photocatalysts. The obtained results indicated that the rate of phenol decomposition in the presence of the sample Ag-TiO_2 6.5% is faster than those for commercial Degussa P25. Silver nanoparticles deposited on the titanium dioxide surface can acts as electron-hole separation centers. This results in the formation of Shottky barrier at the metal-semiconductor contact region, which improves the charge separation and thus enhances the photocatalytic activity of TiO_2. In contrast, at the silver amount above its optimum, the silver nanoparticles can also act as recombination centers, which results in decreasing the photocatalytic activity of TiO_2 [18]. Sano et al. [19] observed that the increase of silver amount resulted in Ag aggregation leading to decrease in photoactivity.

The photodegradation efficiency under visible light increased with the increase in the silver loading up to 6.5 mol % and then decreased. The rate constant value increased with the increase in silver loading up to 6.5 mol% and then decreased (see Fig.3). Thus, it was observed that optimum silver loading for this preparation method was 6.5 mol.%. According to the literature data, the fade of the photoreaction rate at higher metal loading can be accounted for the so-called "screening effect" previously described for Pt/TiO_2, Ru/TiO_2 and Cu/TiO_2 systems used for photocatalytic hydrogen production from water (the deposited silver makes part of the photocatalyst surface less accessible for photons) [20].

Our results are in good agreement with others. Seery et al [21] observed 6 to 50% improvement in visible light photocatalytic degradation of model dye (rhodamine 6G) in the presence of Ag-TiO_2 prepared by photocatalytic reduction of Ag at the TiO_2 surface and by direct calcination of sol-gel material. The rate of degradation of a model dye increased from 0.06 min^{-1} for pure TiO_2 to 0.34 min^{-1} for 5 mol.% Ag-TiO_2. It was attributed to the increasing visible absorption capacity due to the presence of silver nanoparticles [21]. Dobosz and Sobczynski [22] and Liu et al. [23] both reported silver deposits improved efficiency of anatase up to 300% for the UV-enhanced photocatalytic oxidation of phenol at silver loadings of 0.5 and 1 wt.%, respectively. Dobosz and Sobczynski [22] found that optimum silver loading amounted to 0.5 wt.%. However, even at low silver deposition (0.06 wt.%) the influence of the metal addition on the initial photoreaction yield is very high – the reaction proceeded more than 2 times faster. For the

optimum Ag loading, the rate rises as much as 3.6 times [19]. Xin et al. [24] found that the Ag-TiO$_2$ photocatalysts with appropriate content of Ag (Ag species concentration is from about 3 to 5 mol.%) possess abundant electron traps and favor the transfer of the electrons to surface Ag^0. As a result, the recombination of photoinduced charge carriers can effectively be inhibited.

3.2. Absorption properties

As a result of modification of titania with silver, Ag/TiO$_2$ powders of different colors and different color brightness were obtained, as shown in Table 1. The samples prepared by TIP hydrolysis followed by silver deposition in microemulsion system occurred from bright to deep yellow color, depending on silver content. The sample prepared by silver deposition at P25 TiO$_2$ was violet. Thus, all modified powders showed LSPR in visible region what has been a typical phenomenon of nanoparticles of noble metals and exemplary spectra are shown in Fig. 3. It is thought that LSPR peak at 380-390 nm in each absorption spectrum is superimposed on light-scattering inducing no photochemical reactions as was recently shown by action spectrum analysis for Au-TiO$_2$ system [25]. It is also known that LSPR can be tuned from the near-UV through the visible region and even into the mid-IR by changing the size and shape of the nanoparticles [25-27]. In this regard, almost the same position of LSPR peaks of as-prepared Ag-TiO$_2$ indicated that the similar size of silver, regardless of used amount of Ag, is deposited at the TiO$_2$ particles during the microemulsion method.

For the sample Ag -P25 6.5%, the violet color of the sample and a very wide LSPR peak (spectrum not shown here) with maximum at 650 nm indicated that larger and/or non-spherical Ag nanoparticles [25-32] are formed at the surface of P-25 by reduction in the microemulsion system. The LSPR peak shift, from 400 through 500 to 600 nm after the change of nanoparticles shape from spheres through pentagons to triangles [30] and from 400 to 560 nm resulting from Ag nanoparticles coalescence from 10-20 nm to 36 nm broad already reported.

Sung-Suh et al. [33] reported characteristics of Ag-TiO$_2$ obtained by sol-gel method using TIP and AgNO$_3$ as a TiO$_2$ and silver precursors, respectively. They found that Ag deposits size varied with the Ag content in the TiO$_2$ nanosol. For the 2 at.% Ag-TiO$_2$ sample, Ag deposits were well dispersed on the TiO$_2$ particles with an average particle size of 2-4 nm. At higher silver contents, formation of large Ag particles (>100 nm) was observed. Thus, microemulsion system seems favorable for the formation of small Ag particles with narrower size distribution independent on silver content in the reaction system.

3.3. XRD analysis

Fig. 4 shows the XRD pattern of pure and doped TiO_2 powders loaded with different amount of silver. Peaks marked "A" and "R" correspond to anatase and rutile phases, respectively. Both crystalline structures (anatase and rutile) appear for pure TiO_2 prepared by microemulsion method followed by calcination at 450 ℃. Our previous investigation indicated that hydrolysis of titanium (IV) isopropoxide, followed by drying at 80 ℃ and calcination at 350-550 ℃, led to well defined, broad, diffraction peaks corresponding only to the anatase phase [34]. Thus, the microemulsion method affected the crystal structure of obtained TiO_2 – a slight amount of rutile phase appeared for lower calcination temperature. The major phase of all the prepared Ag-TiO_2 is an anatase, regardless of the Ag content. Thus, doping with silver promote the formation of the anatase in preference to rutile. It is well accepted that the concentration of oxygen vacancies strongly influences the rate of the anatase to rutile transformation [10, 35].

The XRD spectra of the Ag-TiO_2 microemulsion, using TIP as TiO_2 precursor, do not show any additional diffraction peak due to silver species. The intensity of the mean silver peak at 37,5° can be masked by the TiO_2 layer, but we did not observe second silver peak at 44° either. Fig. 5 presents the XRD pattern of TiO_2 doped by 6.5 mol.% of Ag prepared by two methods: (1) TIP hydrolysis and subsequent Ag ions reduction in microemulsion system, and (2) silver reduction in the microemulsion system at the surface of P25 Degussa TiO_2 (sample labeled as Ag-P25 6.5%). P25 Degussa TiO_2 particle size is larger than particle size of TiO_2 prepared by the microemulsion method. Thus, XRD peaks of TiO_2 are narrower and thus detection of silver nanoparticles (probably larger than in the case of microemulsion system as was discussed previously according to violet color and LSPR shift towards longer wavelengths) can be much easier.

The crystallite sizes determined from the XRD pattern of the as-prepared photocatalysts are given in Table 1. The average size of anatase crystallites - for Ag-TiO_2 prepared by microemulsion method - was between 8.5 and 11 nm. Thus, for a suitable amount of silver (ca. 2-6 mol %), the grain size was reduced resulting in the increase of the TiO_2 surface area. For sample Ag-P25 6.5% (obtained by Ag deposition at the surface of P25) the average crystalline size was around 29 nm.

3.4. BET surface area and microscopy analysis

Table 1 presents the surface morphological characterization results for the pure and silver doped TiO_2. It can be seen that corresponding to crystalline size decreasing, the specific surface area of Ag-doped TiO_2 increases. The surface area and average crystalline size for

pure TiO_2 are 160 m^2/g and 9 nm, respectively. Sample modified with 6.5 mol.% of Ag has the lowest BET surface area of about 90 m^2/g and the highest average crystalline size of about 11 nm. For other Ag-TiO_2 samples containing from 1.5 to 8.5 mol.% of Ag, the surface area varied from 146 to 157 m^2/g (see Table 1). Thus, except the sample Ag-TiO_2 6.5%, the surface area of pure TiO_2 and Ag-doped TiO_2 obtained by microemulsion method is very similar. Thus, Ag addition, only slightly affects the surface area of powder samples obtained by microemulsion system. Additionally, the surface area for as-prepared Ag-TiO_2 is higher than that of the TiO_2 P25 and than reported by others. Chao et al. [7] reported decrease of the BET surface area for increasing Ag concentration used in sol-gel method. The surface areas of doped TiO_2 powders increased, being 76, 63, and 58 m^2/g, respectively for TiO_2 powders with 2, 4 and 6 mol% Ag doped with respect to that of 45 m^2/g for the pure TiO_2 powder [7]. Hamal and Klabunde [13] described Ag(S,C)-TiO_2 photocatalysts prepared by TIP hydrolysis in the presence of appropriate precursors (AgNO$_3$ and ammonium thiocyanate or thiourea) followed by calcination at 500ºC. The surface area of Ag(S,C)-TiO_2 was 86 and 71 m^2/g for the sample prepared by TIP hydrolysis in the presence of AgNO$_3$/ammonium thiocyanate and AgNO$_3$/thiourea, respectively.

Relations between photoactivity in Vis and UV region versus BET surface area are shown in Table 1. The obtained results indicated that rather other parameters, such as silver presence, cause their enhancement in photoactivity than the surface area. The sample with lower surface area, but containing the optimum amount of silver, revealed the highest photoactivity. However, it is known from the literature that for visible irradiation, the surface area and particle size of titania are not as crucial as the size of noble metal, as was already shown for Au-TiO_2 composites [25].

The morphology of Ag/TiO_2 (Ag-TiO_2_6.5%) composite is shown in Fig. 6. Due to comparable sizes of titania and silver, and strong aggregation of titania it is almost impossible to detect Ag (distinguish Ag from TiO_2) using SEM microscopy (SE STEM), as shown in Fig. 6a. In this regard, ZC and BF STEM images were recorded. Ag nanoparticles are observed as white and dark grey spots on light grey titania in ZC and BF modes, respectively. When too wide a layer of sample is used large white and black spots are detected in ZC and BF modes, respectively, as observed in the center of down images (d and e). The silver nanoparticles are generally spherical in shape. Most of the observed silver nanoparticles deposited at the TiO_2 surface, are in the range from 5 to 10 nm (see Fig. 6d-e.

3.5. XPS analysis

Table 2 shows atomic composition and chemical characters of elements incorporated in the surface layer of pure TiO_2 and Ag-doped TiO_2 prepared in microemulsion system followed by calcinated at 450°C. For some samples, the Ti 2p spectrum could be resolved into two components at binding energies ~458.6 eV and ~457.7 eV and are identified with TiO_2 and Ti_2O_3, respectively [34, 36]. Intensities of the decomposed components suggest that Ti^{4+} is the dominant surface state. In case of TiO_2 modified with 1.5 and 4.5 mol.% of Ag, Ti^{3+} form was not detected. The Ag-TiO_2 6.5% sample contains the highest amount of reduced species in the form of Ti^{3+} ions.

The comparison of oxygen content for pure TiO_2 and Ag-TiO_2 samples, based on XPS spectra for O 1s region, is provided in Table 2. According to the literature data, O 1s peak could be composed of 3 to 5 different species, such as Ti-O bonds in TiO_2 and Ti_2O_3, hydroxyl groups, C-O bond, and adsorbed H_2O [37]. In our investigation four peaks were identified for pure TiO_2 and three peaks were identified for other samples. The first peak at about 532.3 eV was related to oxygen in C-OH bond, the second peak at about 531.2 eV could be assigned to oxygen in Ti-OH bond, the third peak at about 530.2 eV was related to C=O bond and the last peak at about 529.8 eV indicated oxygen in the TiO_2 crystal lattice or oxygen bonded with silver (Ti-O-Ti or Ag-O bonds). The peak assigned as a third peak (BE ~530.2 eV) could be fitted only for pure TiO_2 prepared in microemulsion system. In all Ag-modified TiO_2 samples, as well as in pure TiO_2, we observed the peak attributed to C 1s at around 289-284 eV. In all cases, the C 1s region could be deconvoluted for four to five peaks. It was found that carbon appears as the COOH, C=O, C-OH, and C-C (aromatic and aliphatic) bonds. Carbon content in the surface layer varies from 8.5 to 13.0 at.%, see Table 2. We did not observe correlation between total surface carbon content and visible radiation-induced activity but the sample Ag-TiO_2 6.5%, containing the highest amount of C-C species, clearly showed better activity (see Table 1 and 2). Carbon in the TiO_2 surface layer could originate from organic TiO_2 precursor (TIP), reaction environment (cyclohexane and surfactant) and organic reducing agent.

The presence of silver was confirmed in all the samples modified with $AgNO_3$. The comparison of XPS spectra for Ag $3d_{3/2}$ and Ag $3d_{5/2}$ regions for samples modified with 1.5, 4.5, 6.5 and 8.5 mol.% of Ag are provided in Fig. 7. The XPS spectra of Ag 3d indicated that there are two or three components after deconvolution, attributed to Ag^0 (368.3 eV), Ag_2O (367.6 eV) and AgO (367.05 eV). The silver content in the surface layer increased with the increasing amount of silver precursor used during preparation procedure

and differed from 0.47 to 1.74 at.%. However, increase from 6.5 to 8.5 wt.% of Ag^+ ions in the reaction environment during preparation, did not affect the final silver loading at the TiO_2 surface. Surface content of silver equaled to 1.64 and 1.74 at.% for TiO_2 6.5% and Ag-TiO_2 8.5%_H, respectively. 0.3 at.% of surface silver was in the form of Ag^0 for both samples. Thus, it was not too surprising that photoactivity of both samples is very similar. After 60 min. UV irradiation, phenol was degraded in 85 and 80% for sample Ag-TiO_2 6.5% and Ag-TiO_2 8.5%_H, respectively. Fig. 7 and Table 2 show that for lower concentration, Ag species exist as Ag^0, Ag_2O and AgO, while at high concentration only Ag^0 and Ag_2O coexist at the surface and the amount of Ag^0 species increased to 0.3 at.%. Our observations are in good agreement with others. The presence of Ag^0, Ag_2O and AgO at the TiO_2 surface was reported by others. XPS analysis for Ag-TiO_2 prepared by sol-gel method by Xin et al. [24], confirmed the presence of three peaks for binding energy 367.0 eV, 367.7 eV and 368.2 eV, attributed to AgO, Ag_2O and Ag^0, respectively. It was also found that during photodecomposition of N_2O under UV irradiation on Ag-TiO_2 with different Ag^0 and Ag^+ composition, metallic Ag played crucial role in electron transfer from titania [22].

3.6. Antimicrobial susceptibility testing method (MIC).

It has been well known that silver possesses strong anti-bacterial activities both as Ag nanoparticles and Ag ions. The impact of Ag on microorganism is related to generation of Ag complexes with biomolecules containing sulfur, oxygen and nitrogen such as thiols, carboxylates, amides, imidazols, indoles, and hydroxyls [38].

Determining the MIC values of antibacterial agents is a valuable means for comparing the antibacterial effectiveness of the agents. The MIC values were the lowest concentration of Ag-TiO_2 in aqueous solution that inhibited visual growth after 24 h of incubation. Thus, lower MIC value means higher bioactivity. The minimal inhibitory concentration of microorganism growth for as-prepared Ag-TiO_2 nanocomposites was estimated using bacteria *Escherichia coli* and *Staphylococcus aureus*, yeast *Saccharomyces cerevisiae* and pathogenic fungi belonging to *Candida* family. The effect of silver-loading on MIC value is presented in Table 3. For pure TiO_2 and TiO_2 loaded with 1.5 mol.% of Ag, the inhibition in microorganisms growth was not observed even for photocatalyst concentration below 500 µg/ml. The increase in silver content to 8.5 mol.% caused decreasing of the MIC value related to bioactivity enhancement. The minimal inhibition concentration differed from 6 to 62 µg/ml, depending on microbial strain and Ag concentration (see Table 3).

What was surprising, for two photocatalysts loaded with 8.5 mol.% of Ag prepared by using a different reducing agent (e.g. ascorbic acid and hydrazine), high difference in MIC was observed. The sample prepared by using hydrazine as a reducing agent (Ag-TiO$_2$ 8.5%_H) had much lower bioactivity than the sample prepared with ascorbic acid. The application of hydrazine, stronger reducing agent than ascorbic acid could lead to formation of silver with larger size particles, different silver distribution at the TiO$_2$ surface than in the case of ascorbic acid resulting in a lower active surface and lower bioactivity.

The lower MIC value (the highest bioactivity) was observed for *Saccharomyces cerevisiae* ATCC 9763, *S. cerevisiae* JG and JG CDR1 in the presence of Ag-TiO$_2$ 6.5% sample. It was noticed that silver nanoparticles revealed higher antimicrobial activity against gram-negative bacteria *E. coli* than for gram positive bacteria *St. aureus*. These results were in good agreement with Kim et al. investigation [39]. They have studied antimicrobial activity of silver nanoparticles obtained in aqueous solution. They found that the growth of *E. coli* bacteria were inhibited at the low concentration of Ag nanoparticles (>3nm Ag), whereas the growth-inhibitory effects on *S. aureus* were mild (>33nM Ag). The antimicrobial effects of Ag-TiO$_2$ nanoparticles may be associated with characteristics of certain bacterial species. Gram-positive and gram-negative bacteria have differences in their membrane structure, the most distinctive of which is the thickness of the peptidoglycan layer. We think that lower efficiency of the Ag nanoparticles against *S. aureus* may derive from the difference as a point of membrane structure. To confirm this hypothesis, further comparative study between various gram-negative and gram-positive bacteria species is needed.

Based on the zone of inhibition analysis, shown in Tables 4, it was observed that the Ag-TiO$_2$ particles inhibited the growth of bacteria and yeast. Photocatalyst which exhibited best bioactivity was prepared with 6.5 mol.% of silver. The zone ratios for the Ag-TiO$_2$ particles containing different silver amount in the range from 4,5 to 8,5 mol% were quite comparable. The images of the zone of growth inhibition for *Saccharomyces cerevisiae* and *Escherichia coli* are shown in Fig. 8. The Ag-TiO$_2$ and pure TiO$_2$ nanoparticles are well visible as white spots labeled as: (1) - sample Ag-TiO$_2$ 6.5%; (2) – sample Ag-TiO$_2$ 8.5%; (3) – sample Ag-TiO$_2$ 4.5%; (4) - Ag-TiO$_2$ 1.5% and (7) – pure TiO$_2$. Growth inhibition zones appearing around the spots were lined for easier detection (see Fig. 8).

Liu et al. [40] studied silver-coated TiO$_2$ nanoparticles prepared through the photo-reduction of Ag$^+$ as an antibacterial agent against *Escherichia coli* and *Staphylococcus aureus*. The antibacterial effectiveness of the Ag-TiO$_2$ was evaluated through the

determination of the minimal inhibitory concentration (MIC) of $AgTiO_2$ for each species of bacteria. The MIC values for the Ag-TiO_2, on both *E. coli* and *S. aureus*, were much lower than the MIC values for Ag metal, and quite comparable to the MIC values for $AgNO_3$. A disc diffusion/antibiotic sensitivity test was also performed using the Ag/TiO_2 particles and the results compared with the results obtained for Ag metal, $AgNO_3$ and common antibacterial agents; tetracycline, chloramphenicol, erythromycin, and neomycin. The zone of inhibition diameters for the Ag-TiO_2 particles were found to be comparable with those of the other antimicrobial agents [41].

3.7. Discussion

Sample Ag-TiO_2 6.5% which exhibited best bio- and photoactivity contains about 25.3 at.% of Ti, 64.4 at.% of O, 1.6 at.% of Ag and 13.0 at.% of C atoms. This sample, compared to other samples, has higher amount of Ti^{3+} ions (~1 at.%), silver in Ag^0 form (~0.3 at.%) and carbon (~13 at.%). Thus, photoactivity of this sample could result both from the presence of silver, as well as, from the presence of surface carbon working as a sensitizer and the presence of oxygen vacancies (Ti^{3+} species). The Ag nanoparticles deposited on the surface of TiO_2 could enhance pollutants degradation through: (1) enhancing the electron-hole separation and the subsequent transfer of the trapped electron to the adsorbed O_2 acting as an electron acceptor, (2) extending the light absorption into the visible range and enhance surface electron excitation by plasmon resonance excited by visible light and (3) by modification of the surface properties of a photocatalyst [1, 33, 42-43]. According to the literature, incorporation of carbonaceous species (C-C) occur in highly condensed and coke-like structure, so it could play the role of sensitizer to induce the visible light absorption and response [44-45]. It was found that oxygen vacancy sites (Ti^{3+} sites) promote trapping of holes in the surface region leading to a more efficient charge transfer process. Adsorbed oxygen on the TiO_2 surface scavenges the electrons generating superoxide anions which undergo oxidize organic compounds [46-47]. It was also reported that photo emission from Ag deposited on highly reduced titania surface (Ti^{+3}) leaded to generation of electron-hole pairs at the metal-oxide interface [48]. While, on weekly reduced TiO_2, emission from Ag particles showed characteristics of radiating Mie-plasmon with no electron-hole pair generation.

Over the past several years, a large number of applications of photocatalytic technology have been examined in Japan and the US. One of the important applications of TiO_2 photocatalysts is in the purification of water and air streams [49]. The presence of silver nanoparticles could enhance efficiency of organic pollutants and microorganism removal

from water and air streams. Two proposed Ag-TiO$_2$-based treatment systems for polluted water/air streams are schematically represented in Fig. 9. The Ag-TiO$_2$ thin film (Fig. 9a) or Ag-TiO$_2$-based porous ceramic filter (Fig. 9b) is irradiated with UV-vis light. Water/air flows through the porous filter or over Ag-TiO$_2$ film, where the organic compounds and bacteria adsorb reversibly on the photocatalyst and react. The semiconductor acts as a sensitizer for light-induced redox processes through an electron-hole separation upon absorption of a UV-vis photon. Excited-state electrons and holes can recombine, remain trapped in metastable surface states or react with electron donors and acceptors adsorbed on the TiO$_2$ surface. The latter process initiates a series of oxidation steps conducing to the production of intermediate organic species and final inorganic products such as CO$_2$ and water. Surface available Ag nanoparticles induce the destruction of pathogenic microorganisms. Thus, Ag-TiO$_2$ nanoparticles applied in air conditioning filters could purify and deodorize the interior from volatile organic compounds, which are major air pollutants, emitted largely by industry, transportation, households and also from pathogenic microorganisms. Application of Ag-TiO$_2$-based water/air filters in hospitals, care facilities, public and commercial facilities and schools could reduce the spread of infections and improve the hygienic conditions.

4. Conclusions

The Ag-TiO$_2$ nanoparticles have been prepared using a water-in-oil microemulsion system of water/AOT/cyclohexane. It was found that microemulsion method allowed obtaining Ag-TiO$_2$ nanoparticles with narrow Ag particle size distribution regardless Ag content in the reaction system. XRD and the BET measurements corroborate that these doped materials are made up of the homogeneous anatase crystalline phase and have high surface areas fluctuating from 92 to 158 m^2/g depending on silver amount. It was found that optimum silver loading for microemulsion method amounted to 6.5 mol.% of AgNO$_3$ used during preparation. This sample, compared to other samples, has higher amount of Ti^{3+} ions (~1 at.%), silver in Ag^0 form (~0.3 at.%) and carbon (~13 at.%). Thus, photoactivity probably resulted from the presence of silver (due to enhancing the electron-hole separation and surface plasmon resonance) and the presence of surface carbon working as a sensitizer.

The antimicrobial susceptibility was tested using bacteria *Escherichia coli* and *Staphylococcus aureus*, yeast *Saccharomyces cerevisiae* and pathogenic fungi belonging to *Candida* family. The obtained results showed that bioactivity of Ag-TiO$_2$ differed depending on microbial strain, Ag content and a reducing agent applied during preparation.

This study suggested that silver doped titanium dioxide nanoparticles can be used as effective growth inhibitors in various microorganisms.

References

1   J. Herrmann, J. Disdier, P. Pichat, J. Phys. Chem. 90 (1986) 6028-6034.

2   B. Ohtani, K. Iwai., S. Nishimoto., S. Sato, J. Phys. Chem. B 101 (1997) 3349-3359.

3   V. Iliev , D. Tomova, L. Bilyarska, A. Eliyas, L. Petrov, Appl. Catal. B: 63 (2006) 266–271.

4   N. Halas, MRS Bulletin, 30 (2005) 362-367.

5   X. Yang, L. Xu, X. Yu, Y. Guo, Catal. Commun. 9 (2008) 1124-1129.

6   H. Zhang and G. Chen, Environ. Sci. Technol. 43 (2009) 2905~2910.

7   H. E. Chao, Y. U. Yun, H. U. Xingfang, A. Larbot, J. Eur. Ceram. Soc. 23 (2003) 1457–1464.

8   O. Akhavan, J. Colloid Interface Sci., 336 (2009) 117–124.

9   U.G. Akpan, B.H. Hameed, Appl. Catal. A, 375 (2010) 1− 11

10   Y. Yonezawa, N. Kometani, T. Sakaue, A. Yano, J. Photochem. Photobiol. A 171 (2005) 1–8.

11   K. Kawahara, K. Suzuki, Y. Ohko, T. Tatsuma, Phys. Chem. Chem. Phys . 7 (2005) 3851 − 3855.

12   H. Tran, K. Chiang, J. Scott, R. Amal, Photochem. Photobiol. Sci. 4 (2005) 565-567.

13   D. B. Hamal, K. J. Klabunde, J. Colloid Interf. Sci. 311 (2007) 514–522.

14   W. Zhang, X. Qiao, J. Chen, Mat. Sci. Eng. B 142 (2007) 1–15.

15   R. Inaba, T. Fukahori, M. Hamamoto, T. Ohno, J. Mol. Catal. A: Chem. 260 (2006) 247–254

16   A. Zaleska, A. Zielińska, J. Hupka, (2008) Pat. Appl. P385451

17 A. Zielińska, A. Zaleska, J. Hupka, Proceedings Surfactance and dispersed system in theory and practice, International Scientific Conference, Książ, Poland, 521-524, (22-24 May 2007).

18 A. Sclafani, M. N. Mozzanega, P. Pichat. J. Photochem. Photobiol. A. 59 (1991) 181-189.

19 T. Sano, N. Negishi, D. Mas, K. Takeuchi. J. Catal. 194 (2000), 71-79.

20 A. Sobczyński, J Mol Catal 39 (1987) 43–53.

21 M.K. Seery, G. Reenamole, P. Floris, S.C. Pillai, J. Photochem Photobiol Chem.: 189 (2007) 258–263

22 A. Dobosz A. and A. Sobczynski, Water Res. 37 (2003) 1489-1496.

23 S. X. Liu, Z. P. Qu, X. W. Han, C. L. Sun, Catal. Today 93-95 (2004) 877-884.

24 B. Xin, L. Jing, Z. Ren, B. Wang, H. Fu, J. Phys. Chem. B 109 (2005) 2805-2809.

25 E. Kowalska, R. Abe and B. Ohtani, Chem. Commun., 2 (2009), 241-43

26 E. Kowalska, O. O. Prieto-Mahaney, R. Abe, B. Ohtani, Phys. Chem. Chem. Phys, 2010, DOI: 10.1039/b917399d

27 Y. Xia and N.J. Halas, MRS Bulletin. 30 (2005) 338-344.

28 A. J. Haes, C. L. Haynes, A. D. McFarland, G. C. Schatz, R. P. van Duyne and S. Zou, MRS Bulletin. 30 (2005), 368-375.

29 J. J. Mock, M. Barbic, D. R. Smith, D. A. Schultz, S. Schultz, J. Chem. Phys. 116 (2002) 6755-6759.

30 M. Westphalen, U. Kreibig, J. Rostalski, H. Luth, D. Meissner. Sol. Energ. Mater. Sol. C. 61 (2000), 97-105

31 W. Y. Ma, H. Yang, J. P. Hilton, Q. Lin, L. X. Huang, J. Yao, Opt. Express. 18 (2010)

32 W.-S. Liao, X. Chen, T. Yang, E. T. Castellana, J. Chen, P. C. Cremer, Biointerphases. 4 (2009) 80-85.

33 H. M. Sung-Suh, J. R. Choi, H. J. Hah, S. M. Koo, Y. C. Bae, J. Photochem. Photobiol. A 163 (2004) 37-44.

34 P. Górska, A. Zaleska, E. Kowalska, T. Klimczuk, J. W. Sobczak, E. Skwarek, W. Janusz, J. Hupka, Appl. Catal. B 84 (2008) 440-447.

35 S. Hishita, I. Mutoh, K. Koumoto, H. Yanagida, Ceram. Intern, 1982, 9(2), 61–67.

36 H. Jensen, A. Soloviev, Z. Li, E.G. Sogaard, Appl. Surf. Sci. 246 (2005) 239-249.

37 J. Yu, X. Zhao, Q. Zhao, Thin Solid Films 379 (2000) 7-14.

38 F. Zeng, C. Hou, S. Wu, X. Liu, Z. Tong, S. Yu, Nanotechnology, 18 (2007), 1-8

39 J. S. Kim, E. Kuk, K. N. Yu, J.-H. Kim, S. J. Park, H. J. Lee, S. H. Kim, Y. K. Park, Y. H. Park, C.-Y. Hwang, Y.-K. Kim, Y.-S. Lee, D.-H. Jeong, M.-H. Cho, Nanomedicine: Nanotechnology, Biology, and Medicine 3 (2007) 95– 101.

40 Y. Liu, X. Wang, F. Yang, X. Yang, Micropor. Mesopor. Mat. 114 (2008) 431-439.

41 J. Keleher, J. Bashant, N. Heldt, L. Johnson and Y. Li, World J. Microbiol. Biotechnol. 18 (2002) 133–139.

42 A. Henglein, J. Phys. Chem. 83 (1979) 2209-2216.

43 J. Disdier, J.M. Herrmann, P. Pichat, J. Chem. Soc., Faraday Trans. I 77 (1981) 2815– 2826.

44 C. Lettmann, K. Hildenbrand, H. Kisch, W. Macyk, W.F. Maier, Appl. Catal. B 32 (2001) 215-227.

45 Y. Tseng, C. Kuo, C. Huang, Y. Li, P. Chou, C. Cheng, M. Wong, Nanotechnology 17 (2006) 2490-2497.

46 G. Lu, A. Linsebigler, J.T. Yates Jr., J. Phys. Chem. 99 (1995) 7626-7631.

47 E. Wahlstrom, E.K. Vestergaard, R. Schaub, A. Ronnau, M. Vestergaard, E. Lægsgaard, I. Stensgaard, F. Besenbacher, Science 303 (2004) 511-513.

48 N. Nilius, N. Ernst, H.-J. Freund, Chem. Phys. Lett., 349 (2001) 351-357.

49 A. Fujishima and X. Zhang, C.R. Chimie 9 (2006) 750-760.

Table 1. Characteristics of pure TiO_2 and TiO_2 doped with 1.5 to 8.5 mol.% of silver prepared in w/o microemulsion

Table 2. Atomic composition of $Ag-TiO_2$ photocatalysts

Table 3. Minimum inhibitory concentration (MIC) of Ag-doped TiO_2 for microbial growth (bacteria and fungi). MIC values were determined in the YNBG or TSB medium by a serial dilution method.

Table 4. Zone of microorganism's growth inhibition for $Ag-TiO_2$ nanoparticles

Table(s)

Photocatalyst name	Ag content (mol. %)	Reducing agent	Sample color	Phenol degradation rate constant under UV ($\lambda <$ 400nm) k (min^{-1})	Phenol degradation rate constant under visible light ($\lambda >$ 400nm) k (min^{-1})	BET surface area (m^2/g)	Crystallite size (nm)
pure TiO$_2$	0	none	white	0.003	0.001	160	9
Ag-TiO$_2$ 1.5%	1.5	ascorbic acid	bright yellow	0.003	0.003	157	8.5
Ag-TiO$_2$ 4.5%	4.5	ascorbic acid	yellow	0.017	0.002	146	9.5
Ag-TiO$_2$ 6.5%	6.5	ascorbic acid	yellow	0.023	0.07	92	11
Ag-TiO$_2$ 8.5%	8.5	ascorbic acid	deep yellow	0.02	0.001	148	9
Ag-TiO$_2$ 8.5%_H	8.5	hydrazine	yellow	0.015	0.003	158	8
P25 Degussa	0	none	white	0.018	0.001	59	20[b]
Ag -P25 6.5%	6.5	ascorbic acid	violet	0.027	0.001	45	29

[a] determined as phenol degradation efficiency after 80 min. irradiation
[b] particle size provided by manufacturer

Table(s)

Sample name	Ti content (at. %)			O content (at. %)					Ag content (at.%)				C content (at.%)				
	Σ Ti	Ti^{4+} (458.6 eV)	Ti^{3+} (357.7 eV)	Σ O	C-OH (532.3 eV)	Ti-OH, C=O (531.2 eV)	C=O (530.2 eV)	Ti-O-Ti, Ag-O (529.8 eV)	Σ Ag	Ag-Ag (368.3 eV)	Ag_2O (367.6 eV)	AgO (367.05 eV)	Σ C	-COOH $-CO_3$ (288.6 eV)	C=O (286.8 eV)	C-OH (286.0 eV)	C-C (284.8 284.1 eV)
pure TiO_2	**15.92**	15.44	0.48	**73.43**	3.52	7.07	12.99	49.85	**0**	0	0	0	**10.65**	1.17	2.12	3.47	3.89
Ag-TiO_2 1.5%	**22.81**	22.81	0	**67.8**	4.23	6.7	0	56.87	**0.47**	0.1	0.33	0.04	**8.91**	1.13	0	1.66	6.12
Ag-TiO_2 4.5%	**25.92**	25.92	0	**64.64**	3.34	7.99	0	53.31	**0.97**	0.17	0.71	0.09	**8.47**	0.75	0	1.69	6.03
Ag-TiO_2 6.5%	**25.33**	24.28	1.05	**60.03**	3.05	7	0	49.98	**1.64**	0.30	1.34	0	**13.0**	0.79	0.46	1.59	10.16
Ag-TiO_2 8.5%_H	**20.9**	20.01	0.8	**64.59**	2.44	6.4	0	55.75	**1.74**	0.31	1.43	0	**12.78**	1.5	0	2.43	8.85

Microbial Strains		MIC (µg/ml)					
		Pure TiO_2	TiO_2 1.5%	TiO_2 4.5%	TiO_2 6.5%	TiO_2 8.5%	TiO_2 8.5%_H
Yeast	*Candida albicans* ATCC 10231	> 500	> 500	31	8	16	500
	Candida glabrata DSM 11226			31	62	16	250
	Candida tropicalis KKP 334			16	62	16	250
	Saccharomyces cerevisiae ATCC 9763			31	8	16	250
	Saccharomyces cerevisiae JG			16	8	16	250
	Saccharomyces cerevisiae JG CDR1			16	8	16	250
Bacteria	*Escherichia coli* ATCC 10536			31	31	16	31
	Staphylococcus aureus ATCC 6538			62	31	31	62

Microbial Community	Zone of inhibition for Ag-TiO$_2$ nanoparticles, diameter of zone (mm)						
	Pure TiO$_2$	TiO$_2$ 1.5%	TiO$_2$ 4.5%	TiO$_2$ 6.5%	TiO$_2$ 8.5%	TiO$_2$ 8.5%_H	DMSO
Candida albicans ATCC 10231	-	11	12	13	11	10	-
Candida glabrata DSM 11226	-	13	14	15	15	11	-
Candida tropicalis KKP 334	-	11	14	15	15	14	-
Saccharomyces cerevisiae ATCC 9763	-	12	13	18	13	10	-
Saccharomyces cerevisiae JG	-	13	14	17	15	10	-
Saccharomyces cerevisiae JG CDR1	-	14	14	17	15	10	-
Escherichia coli ATCC 10536	-	20	14	15	20	12	-
Staphylococcus aureus ATCC 6538	-	15	19	16	19	11	-

Figure(s)

Figure 1. Schematic illustration of the Ag-TiO$_2$ nanoparticles preparation method in AOT reverse micelles

Figure 2. Efficiency of phenol photodegradation in the presence of the TiO$_2$ loaded with 1.5 to 8.5 mol.% of silver and pure TiO$_2$ as a reference sample: a) in the presence of ultraviolet radiation (400>λ>250 nm), and b) under visible light (λ>400 nm). Experimental conditions: C$_o$=0.21 mM, m (TiO$_2$)=125 mg, T=10°C, Q$_{air}$=5 l/h

Figure 3. DR spectra of Ag-TiO$_2$ samples loaded with 1.5 to 6.5 mol.% of silver

Figure 4. XRD patterns of silver doped titanium dioxide nanoparticles

Figure 5. Comparison of XRD patterns for TiO$_2$ loaded with 6.5 mol.% of Ag: prepared by simultaneous TTIP hydrolysis and Ag$^+$ ions reduction in microemulsion system (sample Ag-TiO$_2$ 6.5%) and by Ag$^+$ ion reduction in the presence of P25-TiO$_2$ in the microemulsion system (sample Ag-TiO$_2$ 6.5%_Degussa P25)

Figure 6. STEM images of Ag-TiO$_2$_6.5% (sample A): SE-(a), ZC- (b and d) and BF- (c and e) modes for two views: upper and down images

Figure 7. Ag 3d XPS spectra for: a) sample Ag-TiO$_2$ 1.5%, b) sample Ag-TiO$_2$ 4.5%, c) sample Ag-TiO$_2$ 6.5%, and d) sample Ag-TiO$_2$ 8.5%_H,

Figure 8. Zone of inhibition for pure TiO$_2$ and Ag-TiO$_2$ nanoparticles, (1) – sample Ag-TiO$_2$ 6.5%; (2) – sample Ag-TiO$_2$ 8.5%; (3) – sample Ag-TiO$_2$ 4.5%; (4) – sample Ag-TiO$_2$ 1.5% and (7) – pure TiO$_2$

Figure 9. Photodegradation systems for polluted water and air streams: a) Ag/TiO$_2$-based porous ceramic filter for polluted water/air treatment; and b) bacteria and volatile organic compounds (VOC) sorption and degradation on an irradiated Ag/TiO$_2$ film
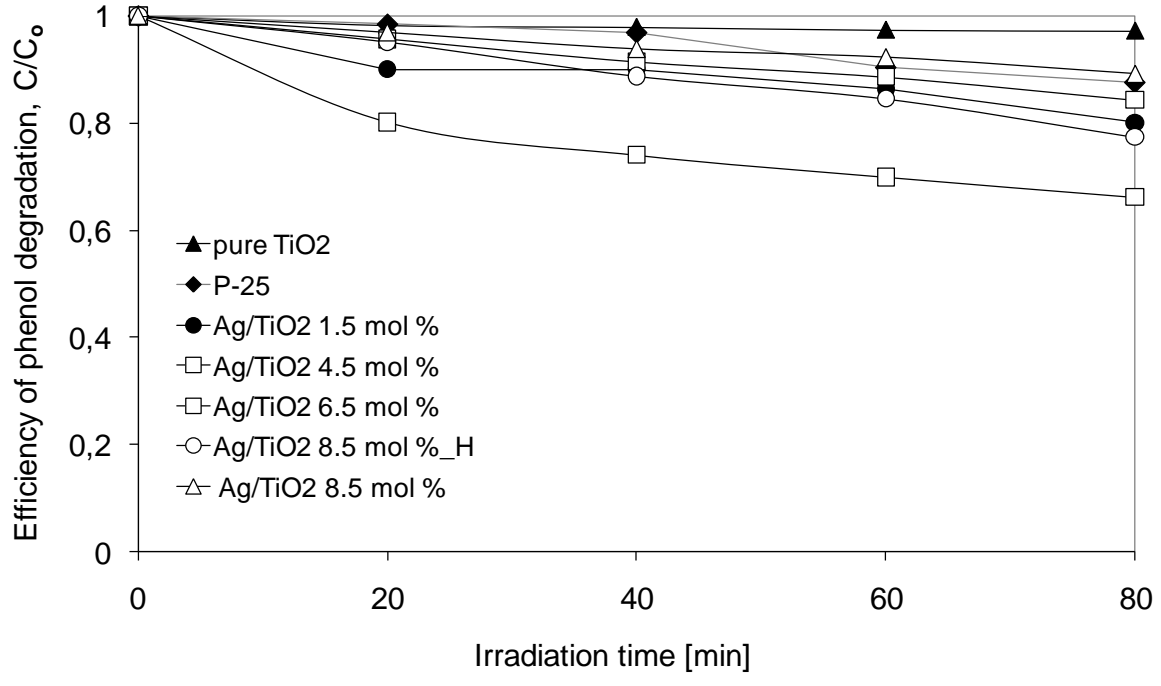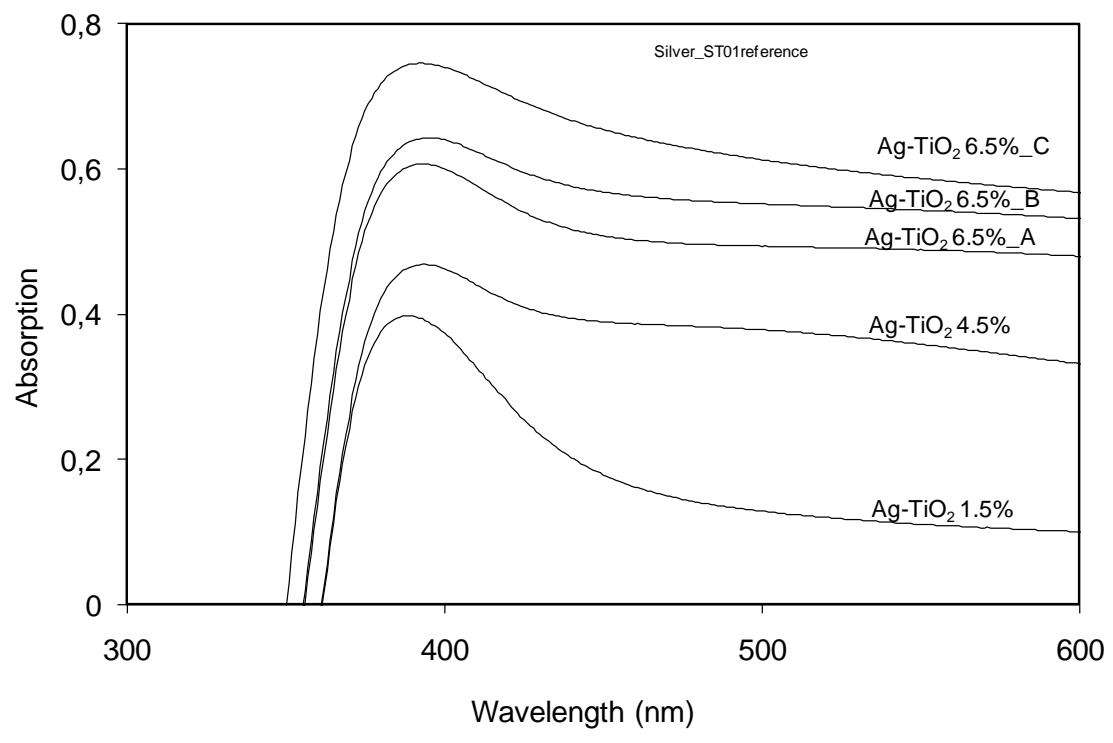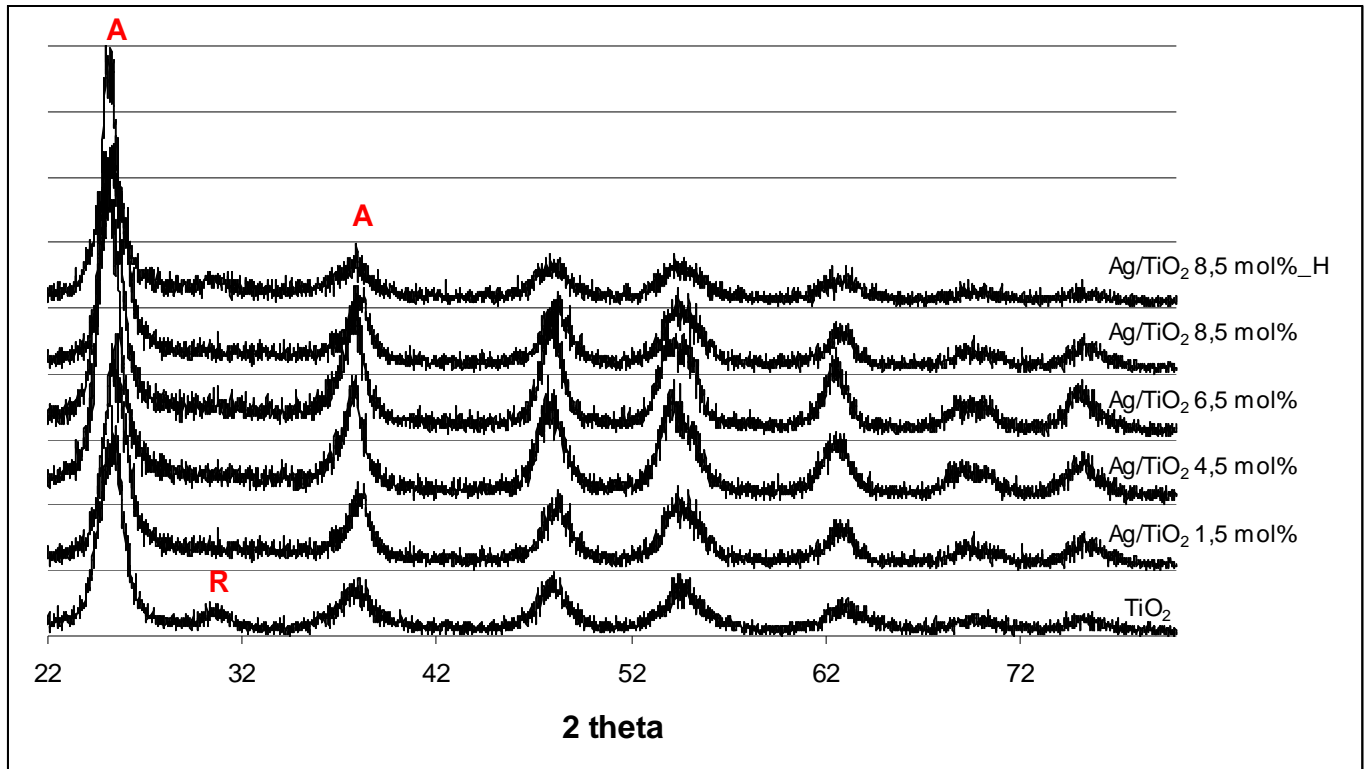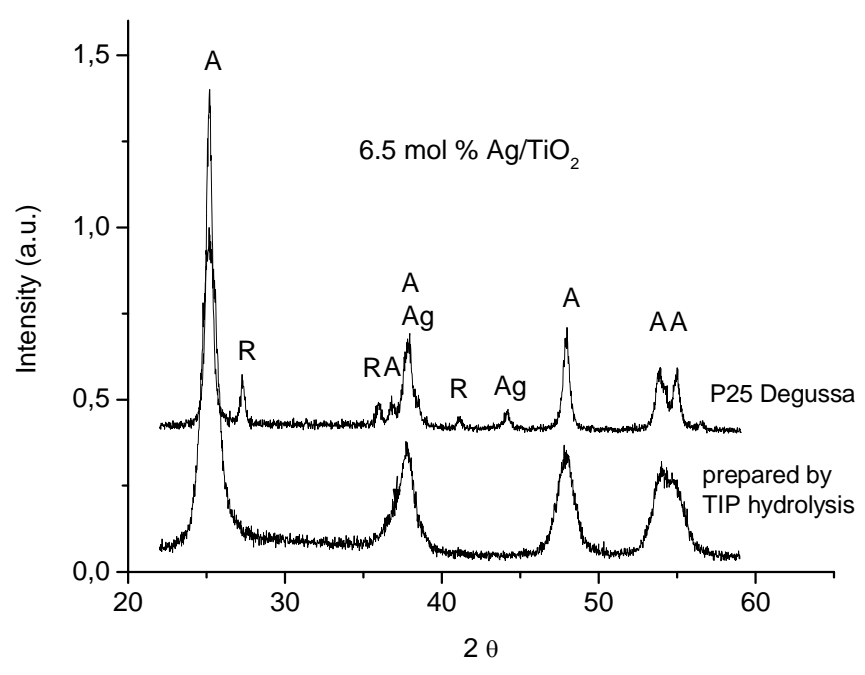
Figure(s)

a)

b)

Figure(s)

Figure(s)

Figure(s)

Figure(s)

Zones of inhibition

Saccharomyces cerevisiae ATCC9763

Escherichia coli ATCC 10536

Figure(s)

a)

VOC in air

UV / VIS

Bacteria in air

Bacteria on surface

CLEAN AIR

Ag/TiO$_2$ film

Surface Ag nanoparticles

b)

Organic compounds in water/air stream

UV / VIS

Bacteria in water/air stream

Ag/TiO$_2$ - based ceramic filter

Clean water/air stream